Epoxy Based Ink as Versatile Material for Inkjet-Printed Devices

Malo Robin,[#,†,‡] Wenlin Kuai,[#,†] Maria Amela-Cortes,[‡] Stéphane Cordier,[‡] Yann Molard,[‡] Tayeb Mohammed-Brahim,[†] Emmanuel Jacques,[†] and Maxime Harnois[*,†]

[†]Université Rennes 1, Institut d'Électronique et des Télécommunications de Rennes, UMR CNRS 6164, Département Microélectronique & Microcapteurs, Campus de Beaulieu, 35042 Rennes Cedex, France

[‡]Université Rennes 1, UMR Institut des Science Chimiques de Rennes, UR1-CNRS 6226, Campus de Beaulieu, CS 74205, 35042 Rennes Cedex, France

Ⓢ Supporting Information

ABSTRACT: Drop on Demand inkjet printing is an attractive method for device fabrication. However, the reliability of the key printing steps is still challenging. This explains why versatile functional inks are needed. Epoxy based ink described in this study could solve this critical issue because it can be printed with low drawbacks (satellites droplets, long-lived filaments, etc.). Moreover, a wide concentration range of solute allows the fabrication of films from thin to high aspect ratio. Optimizing experimental parameters (temperature, overlap) and ink composition (single or cosolvent) is useful to tune the film profile. As a result, many shapes can be obtained such as donuts or hemispherical caps for a droplet and smooth or wavy shape for a thin film. This study demonstrates that epoxy based versatile ink can be used in numerous fields of applications (organic electronics, optics, sensors, MEMS, etc.). To prove this assertion, organic field effect transistors and light emitting films have been fabricated.

KEYWORDS: epoxy based inks, jettability, thin films drying, organic field effect transistors, phosphorescent thin films
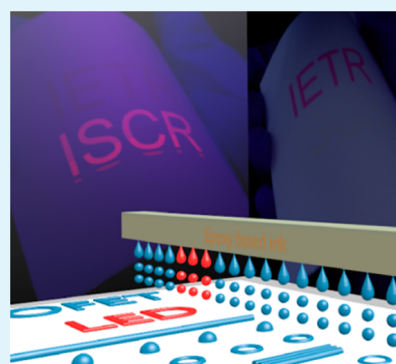
1. INTRODUCTION

Drop on Demand (DoD) inkjet printing technology has gained interest in new application fields such as ceramics,[1,2] biotechnology,[2,3] organic light emitting devices,[2,4] field effect transistors,[2,5] or solar cells.[2,6] This technique allows the deposition of a very small amount of functional material (1−100 pL) at high throughput and high accuracy on various kinds of substrates.[7] These advantages offer new perspectives and promote the development of printable functional materials such as nanoparticles, conducting polymers, and insulators.

The rheological properties of inks have a strong impact on the jetting behavior. Inappropriate ink leads to unstable droplet formation essentially due to nozzle clogging, long-lived filament, and satellite droplets. As a consequence, device reliability suffers from these drawbacks. The partial drying of the first jetted drop also called "first drop problem" at the orifice occurs at nozzle clogging especially when low boiling point solvent ink is used.[8] When printing a highly viscous or high-molecular-weight ink (>500 kDa for a polymer ink), the created droplet is followed by a long filament which can stay attached to the nozzle.[9] Firing voltage is a way to adjust the waveform and may help to solve the liquid filament problem. However, it may cause another problem: undesirable satellite droplets. It has been shown that unstable satellite droplets dramatically do not fall down through the same axis as the main droplet and play a crucial role on the pattern definition.[10]

Patterns formation on the substrate is another key step to evaluate the printing process and consequently the ink quality. Ink is often formed by solid material dispersed in liquid. A droplet deposited on the surface is submitted to a drying mechanism leading to nonuniform film formation, caused, for instance, by the so-called "coffee stain effect".[11]

Considering all the reports of drawbacks in the literature, ink engineering that fits the printing process requirements remains a challenge to overcome. The inkjet printing process is composed of two main steps as described above: jettability and film formation, which must be carefully understood to evaluate if an ink is appropriate.

The aim of this study is to show that epoxy based ink (Su-8), presented in the first section, is an appropriate functional ink for DoD technology. The second section will focus on the viscosity range of printable ink and experimental conditions to optimize the jettability. The third section will describe drying mechanism of a droplet and thin film formation obtained by droplets coalescence. The fourth section reports unprecedented applications with Su-8 based ink: printed organic field effect transistor (OFET) and photoluminescent hybrid thin films.

2. RESULTS AND DISCUSSION

a. Epoxy Based Ink. *i. Promising Processing Properties.* Over these past 5 years, very few studies report on the use of Su-8 (epoxy based ink) inkjet printing process.[20−22] We wish here to give an overall understanding of epoxy based ink (Su-8)

printing parameters to define various kinds of geometric patterns useful for device applications.

Un-cross-linked Su-8 2000 series photoresist (Bisphenol A Novolak epoxy) is an oligomer formed of eight benzene rings and eight epoxy groups with low molecular weight (around 7 kDa) diluted in cyclopentanone.[12] Concerning the printing requirement, Su-8 based ink can take benefits from its low molecular weight to improve its jettability behavior. One could notice that Su-8 polymerization is performed under UV light and after the jetting that enables easy drop ejection (small molecule) and good chemical resistance.

ii. Promising Physical Properties. Over the last 20 years, numerous studies have been realized on Su-8 photoresist leading to a complete state of art paving the way for extending its use as a functional ink. Focusing on optical application, Su-8 is transparent above 365 nm exhibiting low propagation losses and is used in waveguides.[13,14] Su-8 also has an interesting Young modulus for MEMS achievement.[15] Moreover, its insulating properties in microfluidic chips have been also reported,[16] as well as its interesting high-breakdown electric field allowing the fabrication of OFET.[17] Wetting properties combined to microfabrication technology allow the fabrication of superhydrophobic surfaces.[18] Other publications deal with the possibility to blend Su-8 with other materials such as solids.[19] Those attractive physical properties already extensively reported in the literature combined to printing technology will permit an extensive use of epoxy based ink.

b. Jettability. Understanding the droplet generation mechanism (Jettability) is an essential step to demonstrate ink versatility. The idea developed in this section consists of defining jettable bounds (printable windows) of epoxy based ink system. Indeed, inside the printable window, optimized jetting conditions will lead to easily tune the droplet velocity and volume leading to an accurate printing.

Jettability is complex and governed by inertial, viscous, and surface tension forces. Dimensionless numbers including Reynolds (Re), Weber (We), Capillary (Ca), and Z number characterize the droplet formation process.[23]

$$Re = \frac{\text{inertial force}}{\text{viscous force}} = \frac{\rho v d}{\eta} \tag{1}$$

$$We = \frac{\text{inertial force}}{\text{surface tension}} = \frac{\rho v^2 d}{\sigma} \tag{2}$$

$$Ca = \frac{\text{viscous force}}{\text{surface tension}} = \frac{\eta v}{\sigma} \tag{3}$$

$$Z = \frac{\sqrt{\sigma \rho d}}{\eta} \tag{4}$$

where η, σ, and ρ are the viscosity, the surface tension, and the density of the ink, respectively. v is the velocity of the expelled droplet from a nozzle (diameter equal to d).

The Z number eq 4 has been identified as the key parameter linking all the physical criterion to obtain stable droplets jetting.[23] However, a wide range of Z number values have been observed proving that Z number could not be the only parameter to predict ink jettability.[24−26] More recently, studies have led to define printable windows that could be plotted in a coordinate system using the We-Re or Ca-We space.[27,28] In this latter case, systematical experiments following a well-defined methodology have validated the printable windows and could

constitute a reliable reference to qualify epoxy based ink jettability. However, previous study dealt with only pure solvent based ink or nanoparticule based ink. This work goes further than previous work and will demonstrate that low-molecular-weight ink can also match the previously defined printable windows.[28] More precisely, experiments performed in this study will show that low-molecular-weight ink jettability can be described following the same ink design strategy than nanoparticle or pure solvent based ink. In this study, the used methodology can be summed up as follows: optimizing the waveform and then defining the jettability windows using the Ca-We representation. This set of experiments will lead to a complete description of each considered ink.

Depending on application requirements, for instance, a film thickness adjustment, a wide concentration range of epoxy based inks must be characterized from a jettability point of view. In this work, we will study inks with three epoxy based ink dilutions whose physical properties are listed in Table 1 and

Table 1. Physical Parameters of Three Kinds of Epoxy Based Ink and Pure Cyclopentanone Ink Used in This Study[a]

ink	η (cp)	σ (mN m^{-1})	ρ (g mL^{-1})
Epoxy ink 3	15.50	33.20	1.15
Epoxy ink 2	7.50	34.00	1.12
Epoxy ink 1	2.49	35.00	1.07
Cyclopentanone	1.00	33.40	1.00

[a]Nozzle diameter, equal to 21 μm, is extracted from the Dimatix Cartridge datasheet. η, σ, and ρ have been monitored as explained in the Experimental Section.

also presented in the Experimental Section. One could notice that the epoxy oligomer amount mainly tunes viscosity. Moreover, pure cyclopentanone based ink will also be tested as it is the major component of Su-8 2000 series based ink with the lowest ink viscosity used in this study.

i. Waveform Optimization. Figure 1a shows the typical bipolar waveform used in this study. Droplets are formed on positive firing voltage time (t_{dwell}). Negative firing voltage time (t_{echo}) has been fixed at twice of t_{dwell} to avoid residual deformation waves after ejection of each drop. t_{rise} and t_{fall} have been kept as short as possible to not perturb droplet formation and to avoid a large volume of liquid jetting. Jetting is considered stable when the criteria described in the Experimental Section and illustrated in Figure S1 (Supporting Information) are satisfied.

Printable windows in a Ca-We coordinated system can be defined by varying droplet velocity. This can be done by tuning voltage applied on piezoelectric actuators (Figure 1a).[28] However, a prerequisite step is needed and consists of defining optimum jetting conditions for each positive firing voltage time value (t_{dwell}). Thus, this step is performed by varying nozzle pressure (for each t_{dwell}) and allows covering all the printable windows.[28] Moreover, local optimized t_{dwell} values are deduced from momentum versus t_{dwell} plot (Figure 1b) and correspond to the local maximum of momentum values. Momentum (i.e., velocity × mass product) results from droplet volume and mass measurements performed by using stroboscopic vision equipment during jetting.

Results reported in Figure 1 b show that momentum is strongly impacted by t_{dwell}. We found a wide range of printable conditions (until t_{dwell} equal 150 μs) for the three tested inks in this study. Indeed, such results have been successfully obtained
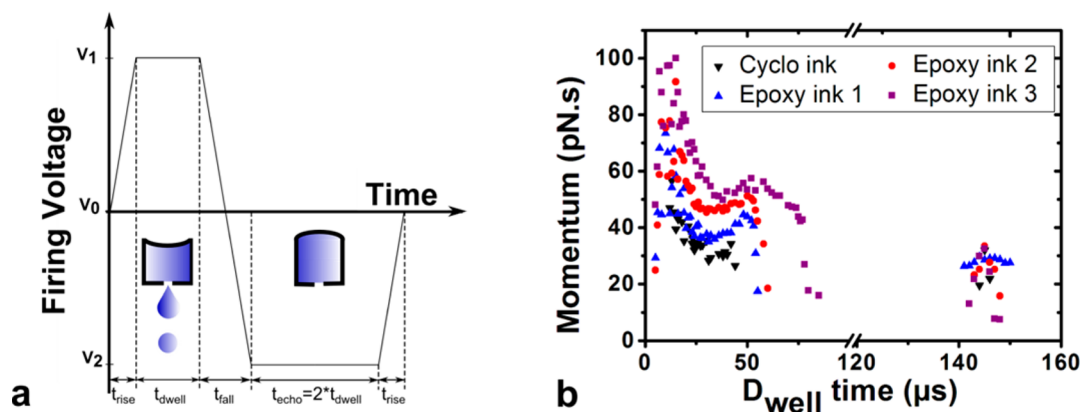
Figure 1. (a) Typical bipolar waveform. (b) Momentum evolution versus dwell time for each ink. Data related to mass and velocity are reported in Figure S2.

by defining optimum jetting conditions. These results go further than the results of Fakhouri et al.[29] based on only one ink without using optimum jetting conditions.

As expected, all the ink systems show the same behavior when keeping the amplitude waveform constant and varying t_{dwell}. Local maximum momentum values are observed at t_{dwell} $\sim$18 μs, $\sim$50 μs, and $\sim$145 μs. Moreover, optimized t_{dwell} can be determined and Ca-We values can be explored for all the considered ink.

ii. Jettability Windows Exploration. As shown in Table 1, viscosity is the relevant parameter of this study (σ and ρ did not vary significantly and d has been kept constant). Ca-We parameter space is used to highlight the impact of viscous and inertial forces on jettability (eqs 2 and 3). This representation allows minimizing the surface tension effect. Inertial forces are mainly governed by velocity that can be explored by tuning the amplitude of pulse waveform at optimized t_{dwell}.

Using experimental data on obtained velocity, rheological parameters (Table 1) and eqs 2, 3, and 4, Weber as a function of Capillary (We versus Ca) is plotted for all the tested functional inks (Figure 2).
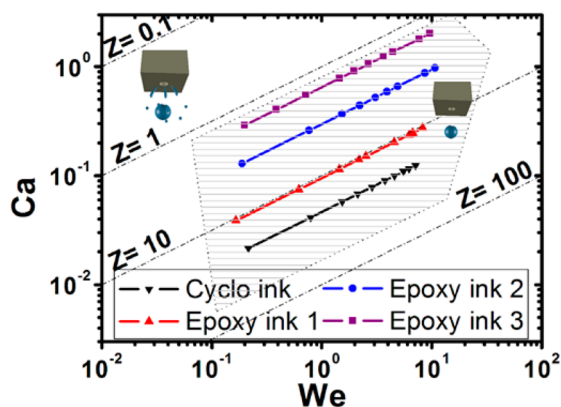
Figure 2. Inkjet qualification strategy represented in a Capillary number (Ca) -Weber number (We) coordinated system of the printable inks tested. For each ink, each data point reports a printable condition corresponding to a different velocity (SI Movie 1). Hatched area: The printable window defined by Subramanian.[28] Scheme inside the hatched area illustrates well-defined drop jetted from a nozzle. Scheme outside the hatched area illustrates inappropriate jetting conditions (i.e., main drop plus additional satellites droplet).

The printable window experimentally defined using solvent based ink and nanoparticule based ink is also added to the graphics. Low Z values (below the low limit of printable windows) and high Z values correspond to epoxy based ink with high and low viscosity, respectively. Outside the printable window, the considered ink does not satisfy the jettable criterion described in the Experimental Section. For instance, at low Ca and We no droplet can be jetted, and at high Ca and We, jetting leads to undesirable satellite droplets (Figure S1 and Movie S1).

Results reported on Figure 2 show that cyclopentanone and epoxy ink 3, which are the lowest and the highest tested viscosities, respectively, are the printability bounds. This interesting set of experiments demonstrates that epoxy based inks match the same printable windows than the one defined using nanoparticule based ink or pure solvent based ink. It means that ink based on low-molecular-weight components (e.g., epoxy base ink) shows stable printing behavior over a large range of printing conditions.

Data related to cyclopentanone reported in Figure 2 correspond to high Z values that are far away from the lower printability limits defined by the printable window ($Z = 60$). This result shows that cyclopentanone is a convenient solvent for inkjet printing technology. As a consequence, very high epoxy dilution in such solvent could be performed to obtain very low film thickness. One could notice that another interesting asset of cyclopentanone printability relies on its use as ink to locally etch Su-8 in order to achieve via for electrical interlayer connections. This concept has already been published using ethanol ink to etch poly(4-vinylphenol) films.[30]

In summary, following an ink design strategy is suitable for understanding the jetting behavior of an ink. Indeed, each ink has specific properties (e.g., for nanoparticle based ink: nanoparticle size, concentration, solvent used, etc.) that must be tuned to be printable. This work demonstrates that low-molecular-weight ink can also fulfill the printing requirements using a rheological properties adjustment. Moreover, for the first time, epoxy based ink has been carefully studied proving its versatility from the jetting point of view. The next section will focus on thin film formation, using one jetting condition for each epoxy based ink.

c. Thin Film Formation. When a mixture of liquid and solid is deposited on a surface, complex drying mechanisms compete and strongly affect the patterns definition; so, these mechanisms need to be described for each considered ink.
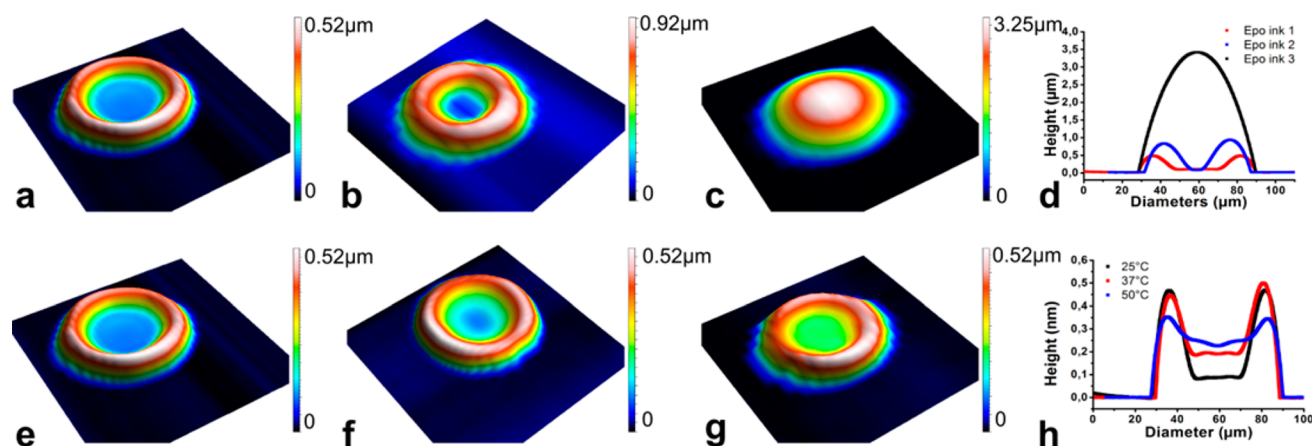
Figure 3. 3D pictures and profiles extracted along diameters of a single droplet. Morphological behavior of different epoxy based inks: (a) Epoxy ink 1, (b) Epoxy ink 2, (c) Epoxy ink 3, and (d) corresponding two-dimensional profiles. Substrate temperature for Epoxy based ink 1: (e) room temperature, (f) 37 °C, and (g) 50 °C; (h) corresponding two-dimensional profiles.
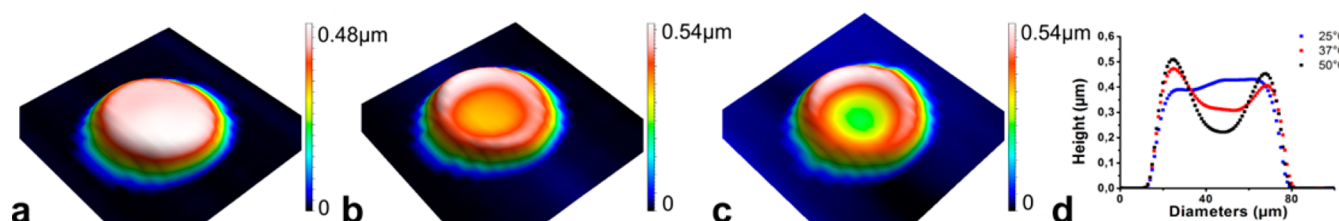
Figure 4. 3D pictures and profiles extracted along diameters of single droplet. Morphological behavior of epoxy based ink using cosolvent based ink (cyclopentanone/γ-butyrolactone; 80/20 wt %) deposited at three different temperatures: (a) room temperature, (b) 37 °C, and (c) 50 °C; d) corresponding two-dimensional profiles.

Numerous studies have reported adjusting overlap and printing frequency parameters to avoid stack coins or bulges for a line shape, but from our point of view, not enough studies deal with square-shaped film formation.[31−33] Indeed, regarding many applications, monitoring the surface morphology of square-shaped films is a critical issue. That is why we decided to deeply investigate the experimental parameters that strongly impact the topology aspect (z dimension) of epoxy printed films.

DoD inkjet printing is based on the coalescence of isolated droplets (pixels) to form complex patterns (e.g., square-shaped films). As a consequence, a deep understanding of a single droplet drying behavior is a prerequisite step to controlling square-shaped pattern morphology that is not sufficiently described and consequently still challenging at the present time. As a result, this section is divided into two parts: the first one deals with isolated droplet drying behavior and the second one deals with the thin film formation.

i. Isolated Droplet Drying Behaviors. A constant droplet volume for different concentrations of epoxy based ink is jetted on glass substrate heated at different temperatures. The droplet profiles are extracted after droplet drying and are shown on Figure 3.

At high dilution (low amount of solids) a ring shape is observed (Figure 3a and b). This phenomenon first described by Deegan and known as "coffee stain" is due to the solvent evaporation rate which is greater at the surroundings of the so-called "triple contact line" (the edge of the droplet in contact with air and substrate).[11,34−36] Consequently, when the contact line is pinned, solute transport from the center to the edge is induced by replenish flow, leading to inhomogeneous films

after complete evaporation. Increasing the solute concentration at fixed diameter leads to the increase in profile edge thickness because more material is deposited on the edge. Consequently, above a limit value of epoxy dilution (high amount of solids), a hemispherical profile is obtained (Figure 3c and d) due to a combination of solids concentration and coffee stain effect. In other words, increasing the amount of solids at pinned contact line leads to the thickness increase of the ring formed on the edge until the formation of a dome-shaped pattern as illustrated in Figure 3d.

The ring shape obtained at high ink dilution, unsuitable for many applications, must be avoided. One frequently used solution consists of introducing inward flow inside the droplet, e.g., the Marangoni effect. This study reports the effect of two parameters such as substrate temperature and the use of cosolvent based ink to improve film homogeneity. For highly diluted epoxy-based ink and substrate kept at room temperature, the internal droplet flow is mainly guided from the center to the edge (outward flow). Evaporative cooling of a droplet leads to a temperature gradient along the air−liquid interface because the lengths of the thermal conduction path decrease from the apex to the edge of the droplet.[37] As a consequence, a surface tension gradient is generated and induces an inward flow commonly called the Marangoni flow. Increasing the substrate temperature leads to the surface tension gradient increase enhancing the Marangoni flow. This effect competes with the drying mechanism described by Deegan. Consequently, the solid epoxy ink components are moved mainly in the droplet center, and more homogeneous films are obtained as substrate temperature increases (Figure 3e−h). Increasing temperature beyond 50 °C could be an interesting way to
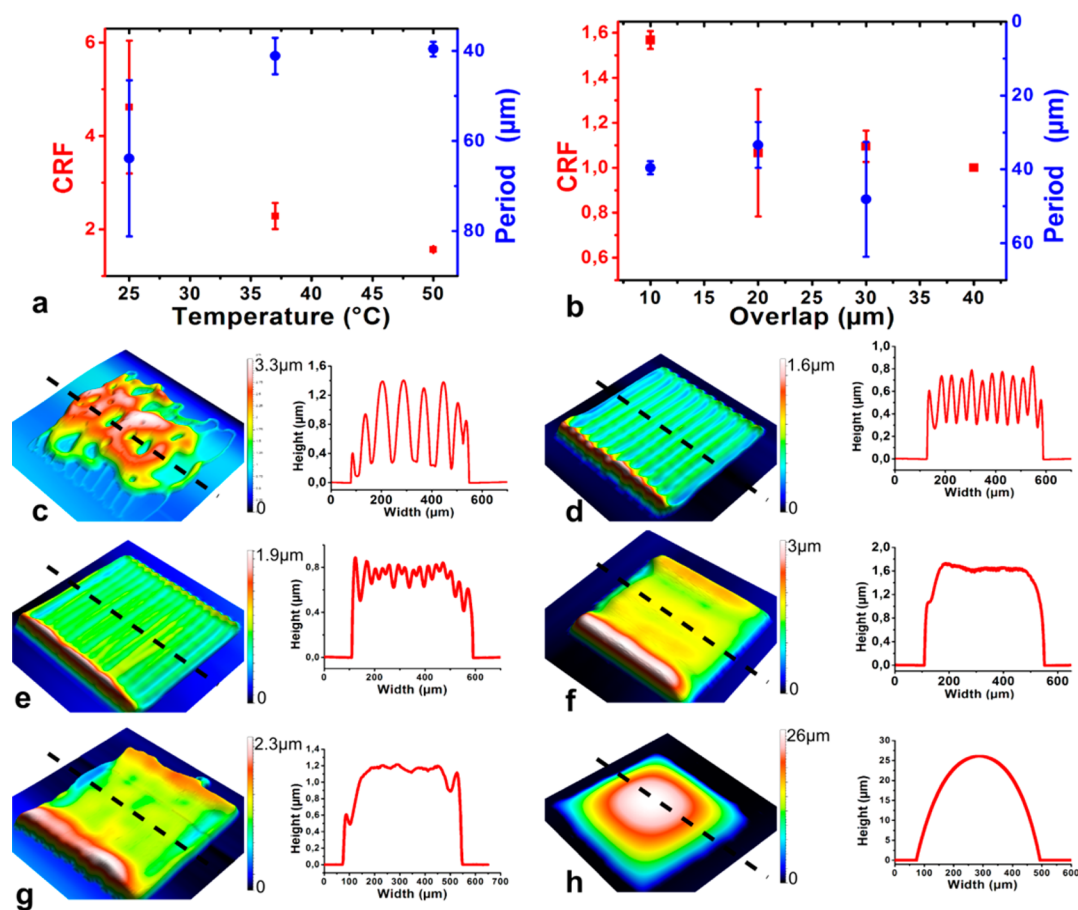
Figure 5. (a) Coffee ring factor (CRF) and wave period (p) versus substrate temperature at fixed overlap; (b) coffee ring factor (CRF) and wave period (p) versus overlap between adjacent droplets at fixed temperature. 3D pictures and corresponding profiles extracted along the dashed lines of 500×500 μm^2 square-shaped thin films. Morphological behavior of epoxy based ink in function of temperature: (c) Epoxy based ink 1 at room temperature and (d) Epoxy ink 1 at 50 °C; In function of overlap: (e) Epoxy ink 1, overlap = 20 μm, and (f) Epoxy ink 1, overlap = 30 μm; In function of ink mixture: (g) Epoxy ink using cosolvent (cyclopentanone/γ-butyrolactone); Varying ink dilution: (h) Epoxy ink 3.

obtain more uniform films but is technically impossible with the printer used in this study. However, a higher substrate temperature could also dramatically lead to nozzle clogging and constitutes an experimental limitation.

To overcome this limitation impact, cosolvent based ink is also studied and resulting profiles are reported in Figure 4.

Epoxy based ink is mixed with γ-butyrolactone (boiling temperature: T_b = 204 °C and surface tension: γ = 40.4 mN· m^{-1}) which is another solvent able to dissolve epoxy molecules.[38] As described above, cyclopentanone (T_b = 130 °C and γ = 29.5 mN·m^{-1}) is the main solvent of epoxy based ink. As reported in Figure 4a and d, homogeneous films are obtained thanks to inward flow at room temperature. For this complex cosolvent based ink composed of a mixture of low and high boiling point, the drying mechanism could be explained as follows: as the droplet evaporation rate is higher at the edge, the mixture composition is imbalanced along the droplet radius, leading to a higher fraction of high boiling point solvent at the edge. This phenomenon leads to a surface tension gradient and consequently Marangoni flow inside the droplet. As a result, a more homogeneous film is obtained thanks to circulatory motion. Additional experiments are carried out on the effect of substrate temperature and reported in Figure 4. Surprisingly, heating the substrate promotes outward flows and the resulting profiles are more convenient to Deegan's theory, i.e., the coffee stain effect (Figure 4b,c,d). A hypothesis could explain this

phenomenon: As cyclopentanone is more volatile than γ-butyrolactone, according to the vapor pressure law versus temperature, the difference of evaporation rate between these two products drastically increases at 50 °C. This phenomenon leads to evaporation of cyclopentanone before complete droplet drying. As a consequence, the evaporation mechanism could be described as follows: First, the two solvents are in the droplet enhancing circulation motion, i.e., Marangoni flow. Then, only γ-butyrolactone remains in the droplet enhancing radial outward flow. This leads to the coffee ring profile.

This additional experiment clearly shows that drying mechanisms are complex. One could notice that solvent ratio must be adjusted versus the drying temperature to obtain the desired profile.

To conclude, on a single droplet drying ("pixel") behavior, results previously described constitute a solid data set allowing the fabrication of multiple profile shapes such as thin or sharp donuts, thin homogeneous films, and high-aspect-ratio hemispherical caps. However, many applications require film formation instead of "pixel". Unfortunately, drying films are less described in the literature. As a consequence, taking benefit from the deep understanding of single droplet drying behavior, the following section will report on the main experimental parameters that control thin film drying behavior.

ii. Thin Film Drying Behaviors. Drying mechanisms are more complex for a film than for an isolated droplet because of
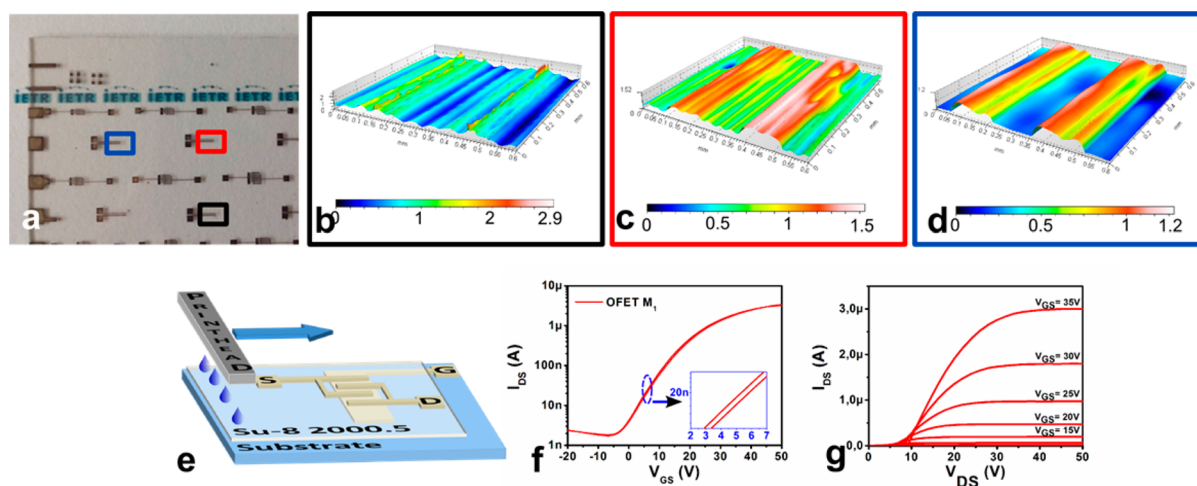
Figure 6. Fabrication and electrical characterization of OFET. (a) Printed drain and source fabricated on printed insulator (epoxy based ink 1): Areas in black, red, and blue squares show M_0, M_1, and M_2 location, respectively. 3D profile showing electrodes and different insulator morphology: M_0, M_1, and M_2 illustrated in (b), (c), and (d), respectively. (e) Bottom gate/bottom contact OFET fabricated by inkjet printing (details are mentioned in experimental part). (f) Transfer characteristics for M_1 and hysteresis shown in inset at V_{DS} = 20 V. (g) Output characteristics for M_1.

the printing sequence described as follows: droplet coalescence along x axis forms one line and line coalescence along y axis forms the film. Tekin et al.[39] used high-molecular-weight based ink (PMMA) to achieve smooth films using multilevel printing layers at relatively low head velocity of about 6.25 mm.s^{-1}. Our study deals with the effects of printing parameters on morphological film behavior (e.g., from wavy to smooth-shaped profiles) at higher head velocity using a monolevel printing technique which fits more with industrial criterions.

So, additional parameters must be taken into account in order to describe the film drying behavior such as printing frequency and overlap between printed droplets. For this study, printing frequency is fixed at 1 kHz corresponding to 35 m.s^{-1} < v_{print} < 50 m.s^{-1} depending on overlapping distance between droplets. For the set of experiments used in this study, overlapping range is chosen in order to obtain smooth line edges. Glass substrate temperature does not exceed 50 °C, which guarantees no nozzle clogging. Different experimental parameters such as substrate temperature, overlap, use of cosolvent based ink, and ink concentration are investigated. Figure 5 shows 3D views and their corresponding profile of 500 × 500 μm^2 square thin films. Two parameters are used to qualify the smoothness of the films. The first one is the periodicity (p) of wavy shape and the other one is the coffee ring factor (CRF) which is the ratio between the maximum and the minimum height of the film for one period. All the measurements are performed on 500 × 500 μm^2 square-shaped films, and calculated values of p and CRF are an average of one profile of the film (Figure 5d,e,f,g: area colored in red shows a higher z height). One could notice that ink excess is observed essentially at the beginning of the patterned area. The phenomenon has already been described in the literature and seems to be due to the pressure difference in the film along the printing direction which is strong enough to pump the liquid at the film start.[31,39,40] For practical applications, this ink excess must be taken into account and must be out of the active area.

Figure 5 shows that extremely different morphologies can be obtained: from disorganized films to thin periodically waved films (PWF) for highly diluted epoxy based ink. At fixed overlap, substrate temperature has a strong impact on CRF and p (Figure 5a). At low temperature, nonuniform films are

obtained as highlighted by high standard deviation of the CRF (Figure 5a and c). Concretely, inhomogeneous and non-reproducible film observed on Figure 5c is unsuitable for applications. As previously described, the increase of substrate temperature enhances inward flow, which seems crucial to obtain well-ordered PWF (low p standard deviation) and reduces p as shown on Figure 5a. These interesting results show that it could be possible to obtain PWF. In addition, the possibility to adjust period and amplitude of films could be useful for optical applications, for instance.

As depicted in Figure 5b, keeping fixed temperature ($T_{substrate}$ = 50 °C) and increasing overlap drastically reduces the CRF and the period until reaching a smooth film (CRF = 1).

For this experiment, drying is governed by outward flow and two mechanisms must be taken into account in order to describe film formation in the pattern center. At low overlap, the film formation must be considered at the microscopic scale (lines). Below an overlap limit, the lines are formed independently of each other and the evolution of the wavy-shaped profile is due to the local coffee ring effect. When the overlap threshold value is reached, there is enough solid on the same surface area (the contact line is pinned) to overcome the coffee ring effect at the local scale. As reported in Figure 5e the lines began to merge.

At high overlap, the film formation must be considered at macroscopic scale (films). Adding material at the pinned contact line leads to the increase of the film thickness bypassing the coffee ring effect (Figure 5f). Note that such results could be obtained with film thickness of about 3 μm, which is 7 times lower than the multilevel layer printing technique.[39]

Cosolvent epoxy based ink is also jetted to form thin films (Figure 5g). As expected, even if the temperature is decreased, more uniform films are obtained than those formed thanks to single solvent based ink with the same overlap between droplets. The ink concentration effect is reported in Figure 5h and f. The increase of solute concentration leads to high aspect ratio hemispherical profiles certainly for the same reasons as previously explained, i.e., increasing solute amount at pinned contact line.

To conclude on the thin films formation, the reported results constitute a solid data set allowing the fabrication of a wide

Table 2. Printed OFET Geometrical and Electrical Parameters[a]

OFET	CRF	W/L (μm/μm)	insulator thickness (max/min in nm)	μ_{FE} (cm^2·V^{-1}·s^{-1})	V_{TH} (V)	SS (V/decade)	I_{on}/I_{off}	V_{DS} (V)
M$_0$	2.3	3800/84	700/300	--	--	--	--	--
M$_1$	1.1	3800/84	1000/900	0.04	17.3	9.69	1.74×10^3	20
M$_2$	1	3800/84	>1600	--	--	--	--	--

[a]M$_0$, M$_1$, and M$_2$ represent the three printing conditions (varying overlap). μ_{FE}, V_{TH}, subthreshold slope (SS), I_{on}/I_{off} ratio are extracted from transfer characteristics.

range of profiles by using single or cosolvent based ink. Tuning experimental parameters such as temperature, overlap, or ink concentration is a useful method to fabricate well-ordered wavy thin films, smooth and hemispherical profiles. These results prove the epoxy based ink versatility and allow more complex device fabrication.

d. Applications. With the benefits of the complete study previously described, many applications can be considered. The next section will describe epoxy based ink potentialities in the fabrication of two unprecedented devices dedicated to OFET and lighting applications.

i. Organic Field Effect Transistors. Fully solution processed OFET on every kind of substrate is a topical issue and is still challenging. Therefore, new insulated functional inks are needed. To date, poly(4-vinylphenol) (PVP) is the most dielectric used for OFET fabrication by inkjet printing, but several drawbacks could be listed. One of them, the curing temperature around 200 °C, is unacceptable for electronics applications on plastic substrates. Indeed, most commonly used plastic substrates (PEN or PET) can be processed at a maximum temperature lower than 200 °C. Consequently, other printable insulating material must be suggested. We are convinced that epoxy based ink is an appropriate functional material due to its excellent film-forming properties as demonstrated in the first part of this work. Moreover, ink shows other interesting properties such as low temperature processing (around 100 °C), good chemical resistance, wettability, low leakage current density, dielectric constant about 3,[41] and high breakdown electric field (evaluated at 3 mV.cm^{-1}).

Results depicted in Figure 6 show that a printed epoxy thin film layer can be used as gate insulator for OFET fabrication.

The optical picture in Figure 6a shows silver ink lines (source and drain electrodes) printed on different epoxy insulating layers morphology (Figure 6b,c,d). These different morphologies (M$_0$, M$_1$, and M$_2$) are obtained by controlling overlap as previously explained. As depicted in Table 2, M$_0$ shows bigger wave amplitude than M$_1$ (higher CRF). As expected, overlap has a strong impact on insulator thickness. As overlap increases, maximum and minimum insulator thickness values increase. Nevertheless, the minimum value is more impacted leading to a strong decrease of CRF.

Only OFET fabricated using M$_1$ is working (i.e., fabrication process described in Figure 6e and in the Experimental Section) with electrical behavior reported in Figure 6f and g. Indeed, OFET fabricated using M$_0$ shows dramatic gate leakage current due to the low minimum insulator thickness leading to failing OFET. Moreover, OFET fabricated using M$_2$ cannot work, at the present time, also because of insulator thickness. We suggest that because of high insulator thickness, the electric field necessary to channel the establishment is too high and consequently leads to failing transistors.

Epoxy based ink versatility allowed us to define an accurate insulator thickness adjustment leading to the fabrication of

OFET with electrical characteristics reported in Table 2. The field effect mobility (0.04 cm^2 V^{-1} s^{-1}) and threshold voltage (17.3 V) values were calculated in the linear regime from the transfer characteristic using the following equation:

$$I_{DS} = \left(\frac{WC_i}{L}\right)\mu(V_G - V_{TH})V_{DS} \tag{5}$$

Output characteristics, are also plotted at different values of gate-source voltage V_{GS} (Figure 6g) showing a modulation of I_{DS} versus V_{GS} (linear and saturation regimes are clearly identified).

Improvement of OFET electrical behavior could be performed by monitoring other parameters such as monitoring electrode morphology,[42] chemical modification of source and drain electrodes, but will not be discussed in the present study.

Moreover, transfer characteristics showing low hysteresis value (500 mV) prove relatively low mobile charge density at the interface between organic semiconductor and printed insulator layer (inset in Figure 6f).

In conclusion, concerning the literature, unfortunately only a few studies deal with full inkjet printing OFET (including polymeric gate insulator) and it is difficult to compare electrical performance reported in this study with others. Focusing on devices achieved using polymeric gate insulator (i.e., independent of processing technics, electrodes material, OSC material), a mobility in the range 0.001−1 has been obtained.[43,44] These original experiments prove that epoxy based inks are an alternative versatile material to achieve OFET devices. Moreover, this study shows that a deep understanding of jettability and morphological behavior is a prerequisite step necessary to achieve more complex devices.

ii. Photoluminescent Thin Film. Octahedral transition metal nanocluster units of general formula [M$_6$L$^i_8$L$^a_6$]$^{2-}$ are strong emitters in the red-NIR region when excited by UV light making them relevant inorganic dyes for applications ranging from biolabeling, lighting and displays (M = Mo, Re, W; a for apical and i for inner; L^i = halogen and/or chacogen; L^a = halogen or functional organic ligand).[45] They are obtained by high-temperature solid-state synthesis as ceramic powders with the A$_x$[M$_6$L$^i_8$L$^a_6$] formula (A = alkali ions, divalent cations (transition metal, rare earth, or alkali earth). In the solid state, the latter are brittle and exhibit a low plasticity limiting their shaping and integration in functional devices. On the other hand, the solubilization of M$_6$ solid state compounds provides [M$_6$L$^i_8$L$^a_6$] building blocks with individual properties (optical, electronic, and redox) that can be further used in nano-architectonics and for the design of functional nanocomposite materials or surfaces.[46−49] Indeed, many works have been dedicated over the past few years to the introduction of inorganic M$_6$ cluster-based building blocks in easy-to-handle organic matrices forming hybrid organic/inorganic nano-composites such as liquid crystals and copolymers. They combined the luminescence properties of the inorganic clusters and the easy shaping of the organic matrices.[50−54] Among this
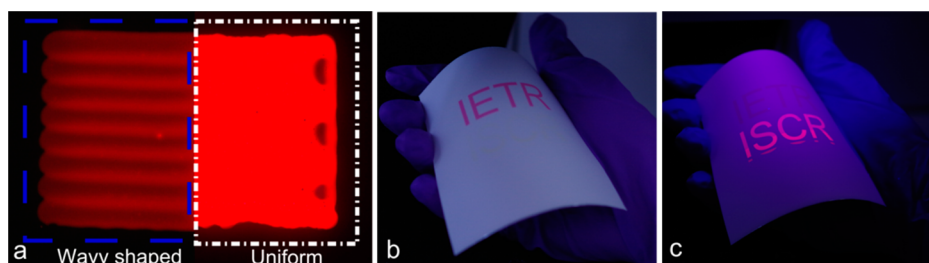
Figure 7. (a) Optical picture of different profiles obtained by varying the overlap parameter during printing. Scale bar is 50 μm. (b) Optical picture showing 10×10 cm^2 square paper substrate. "IETR" is printed with red ink and "ISCR" is printed with cluster/epoxy hybrid based ink. Under room light exposure, nearly only "IETR" is visible. (c) Under 375 nm light exposure, nearly only "ISCR" is visible. See Movie S2.

inorganic nanolightbulb family, the $[Mo_6I_8(OCOC_nF_{2n+1})_6]^{2-}$ ($1 \leq n \leq 3$) cluster unit series appears as the most promising in terms of applicative prospects because of its high efficiency to emit red light. Indeed, quantum yields values up to 1 were reported in the recent literature.[55,56] The $Cs_2Mo_6I_8(OCOC_2F_5)_6$ cluster compound used in this study was synthesized starting from the $Cs_2Mo_6I_{14}$ precursor.[57] We chose this cluster compound to highlight the possibility to mix epoxy based ink with such inorganic nanobuilding blocks and to print the mixture using the process described in the first part of this work.

The mixture contains 5 wt % of the synthesized clusters. Rheological properties of this hybrid ink satisfy the jettability criterions defined in the first section. This point demonstrates the need of a jettability study before device fabrication.

When excited at 375 nm, the mixture presents a large phosphorescence emission band centered on 680 nm, CIE coordinates (x,y) of (0.59, 0.28) and IQE around 0.64. (See Figure S3 for photoluminescence spectrum.) This value of photoluminescence efficiency (IQE) figures is among the best for deep red emitting polymer film containing octahedral metal clusters.[58−60] Note that other kinds of deep red photoluminescent polymer films presenting a better efficiency can be found eventually found in the literature.[61] They are usually based on organic emitters that may suffer from the well-known photobleaching which is not the case for cluster-doped nanocomposites.[62]

Figure 7a shows the red emission of inkjet film printed from the mixture. The printing leads to smooth or wave-shaped films depending on the printing conditions as for epoxy ink alone. The right image of this figure highlights well the uniformity of the film.

Acronyms IETR and ISCR were printed on the same substrate by using usual red ink (Dimatix Fujifilm XL30 Fluid-Red) and mixture ink, respectively. Under room light exposition, only IETR letters were visible. ISCR letters were nearly invisible (Figure 7b). Under 375 nm UV light exposition, the mixed film emits red light and, consequently, the letters ISCR (Figure 7c) are visible.

This very simple example demonstrates the possibility to use epoxy ink mixed with different nanoparticles to fabricate functional films.

3. CONCLUSION

For the first time, a complete study of an epoxy based ink has been reported showing its ability to fit the DoD technics requirements and consequently giving new opportunities to fabricate inkjet-printed devices. Two applications such as organic field effect transistor and functional films (light emitting

thin films here), which have never been described before with this ink, have been carried out to prove it. Moreover, the results obtained from the major printing steps have also confirmed the versatility of this ink. First, the experiments on jettability limit evaluation have shown that the creation of well-defined shaped droplets is possible in a wide range of viscosity including pure solvent. The low molecular weight of the epoxy molecule is certainly helpful to decrease the drawbacks (first drop problem, long-lived filament, satellite droplets, etc.) which are often reported in the literature. Second, the experiments performed on film formation will constitute a useful data set of profiles achievable using this versatile ink. To sum up, optimizing only two ink parameters (dilution and cosolvent) and two printing parameters (substrate temperature and overlap) have led to obtain shapes with tunable aspect ratio (donuts or hemispherical droplets and smooth or well-ordered wavy film). Moreover, we think that the drying mechanism described in this work will be helpful to describe in detail the behavior of other printable materials.

4. EXPERIMENTAL SECTION

a. Jettable Criterion. The jettable criterion is the ability to obtain a droplet at a distance range (Δr) between 800 μm and 1 mm (acceptable working distance for the printer equipment: CERADROP Xseries). Satellite droplets (Figure S1) or tail must be reabsorbed by the nozzle and jettability must be stable for a long time with low droplet misalignment on the substrate ($\Delta x < 5$ μm). All the measurements were performed at 1 kHz jetting frequency. The stroboscopic vision system was used to determine droplet volume and velocity of three ink dilutions.

b. Processing of Epoxy Based ink. Single solvent epoxy based ink has been engineered by using SU-8 2000 series, (MicroChem, Westborough, MA, USA). Su-8 based ink 1 and 2 correspond to the manufacturer reference Su-8 2000.5 and Su-8 2002 photoresists, respectively: Epoxy based ink 3 has been obtained from Su-8 based ink 2 by the evaporation of cyclopentanone (Sigma-Aldrich) until reaching the desired viscosity. All the inks have been jetted without the filtering step.

Cosolvent based ink was engineered by using a mixture of the Epoxy based ink 1 and 20 wt % of γ-butyrolactone (Sigma-Aldrich). Cosolvent based ink surface tension value was 34.2 mN·m^{-1}.

c. Synthesis of $Cs_2Mo_6I_8(C_2F_5OCO)_6$ Octahedral Clusters. *$Cs_2Mo_6I_{14}$.* The synthesis is reported in the literature.[53]

$Cs_2Mo_6I_8(C_2F_5OCO)_6$. To a solution of $Cs_2Mo_6I_{14}$ (1.5 g, 0.52 mmol) in 20 mL of acetone was added a solution of silver pentafluoropropionate (0.935 g, 3.42 mmol) in 10 mL of acetone under argon and in the dark. The mixture was left for 48 h in the dark and then was filtered through a Celite pad. The red solution was then evaporated to yield a red-orange powder. The integrity and purity of the compound were confirmed by ^{19}F-NMR by the presence of only two signals at $\delta = -83$ ppm and $\delta = -120$ ppm, by EDAX and by X-ray diffraction on single crystals.[54]

d. Device Fabrication. Except for the organic semiconducting layer, the OFET devices were fully printed on Corning glass substrate. The substrates were ultrasonically cleaned in acetone and isopropyl alcohol for 10 min. Silver gate electrode (Silverjet DGP 40LT-15C from ANP) was printed on glass substrate using 256 nozzles Q-class printhead (Dimatix) and baked in an oven at 130 °C for 30 min. Then, Epoxy ink 1 was printed using a 16 nozzles cartridge (Dimatix) and baked at 95 °C for 5 min in an oven followed by UV (λ = 365 nm) exposure and baked again in an oven at 95 °C for 5 min. Due to the high hydrophobicity of the insulator, the UV−ozone treatment is needed to increase its hydrophilicity allowing the fabrication of accurate source and drain. Silver source and drain (Silverjet DGP 40LT-15C from ANP) electrodes were printed on a 700-nm-high epoxy layer. Finally, 25-nm-thick organic semiconductor (fullerene C60 Sigma Aldrich) was thermally evaporated as active layer.

e. Characterization. Viscosity and surface tension measurements were monitored using Malvern labpro+ rheometer and Kruss DSA30 equipment, respectively. Profilometry measurements were performed using TENCOR KLA P6 equipment. All the electrical tests were performed in a glovebox using Keithley 2636A and Labview software.

■ ASSOCIATED CONTENT

ⓢ Supporting Information

The Supporting Information is available free of charge on the ACS Publications website at DOI: 10.1021/acsami.5b06678.

> Figure S1. t_{dwell} impact on jettability for: (i) Cyclopentanone; (ii) Epoxy based ink 1; (iii) Epoxy based ink 2; (iiii) Epoxy based ink 3. Figure S2. Mass, velocity, and momentum evolution versus dwell time. Figure S3. Photoluminescence spectrum of Su-8/cluster based ink at λ_{exct} = 370 nm (PDF)
>
> Movie showing droplets jettability for several amplitude voltages on the same printhead (AVI)
>
> Movie showing 10 × 10 cm^2 square paper substrate. Under room light exposure, nearly only "IETR" is visible. (AVI)

■ AUTHOR INFORMATION

Corresponding Author
*E-mail: maxime.harnois@univ-rennes1.fr.

Author Contributions
#Malo Robin and Wenlin Kuai contributed equally to the work. All authors have given approval to the final version of the manuscript.

Notes
The authors declare no competing financial interest.

■ REFERENCES

(1) Derby, B. Inkjet Printing Ceramics: From drops to Solid. *J. Eur. Ceram. Soc.* **2011**, *31*, 2543−50.

(2) Singh, M.; Haverinen, H. M.; Dhagat, P.; Jabbour, G. E. Inkjet Printing—Process and Its Applications. *Adv. Mater.* **2010**, *22*, 673−685.

(3) Medina-Sánchez, M.; Martínez-Domingo, C.; Ramon, E.; Merkoçi, A. An Inkjet-Printed Field-Effect Transistor for Label-Free Biosensing. *Adv. Funct. Mater.* **2014**, *24*, 6291−6302.

(4) Kwak, D.; Lim, J. A.; Kang, B.; Lee, W. H.; Cho, K. Self-Organization of Inkjet-Printed Organic Semiconductor Films Prepared in Inkjet-Etched Microwells. *Adv. Funct. Mater.* **2013**, *23*, 5224−5231.

(5) Avis, C.; Hwang, H. R.; Jang, J. Effect of Channel Layer Thickness on the Performance of Indium-Zinc-Tin Oxide Thin Film Transistors Manufactured by Inkjet Printing. *ACS Appl. Mater. Interfaces* **2014**, *6*, 10941−10945.

(6) Krebs, F. C. Fabrication and processing of polymer solar cells: A Review of Printing and Coating Techniques. *Sol. Energy Mater. Sol. Energy Mater. Sol. Cells* **2009**, *93*, 394−412.

(7) Kang, B.; Lee, W. H.; Cho, K. Recent Advances in Organic Transistor Printing Processes. *ACS Appl. Mater. Interfaces* **2013**, *5*, 2302−2315.

(8) Calvert, P. Inkjet Printing for Materials and Devices. *Chem. Mater.* **2001**, *13*, 3299−3305.

(9) De Gans, B. J.; Kazancioglu, E.; Meyer, W.; Schubert, U. S. Ink-jet Printing Polymers and Polymer Libraries Using Micropipettes. *Macromol. Rapid Commun.* **2004**, *25*, 292−296.

(10) Jang, D.; Kim, D.; Moon, J. Influence of Fluid Physical Properties on Ink-Jet Printability. *Langmuir* **2009**, *25*, 2629−2635.

(11) Deegan, R. D.; Bakajin, O.; Dupont, T. F.; Huber, G.; Nagel, S. R.; Witten, T. A. Capillary Flow as the Cause of Ring Stains from Dried Liquid Drops. *Nature* **1997**, *389*, 827−829.

(12) Hayek, A.; Xu, Y.; Okada, T.; Barlow, S.; Zhu, X.; Moon, J. H.; Marder, S. R.; Yang, S. Poly(glycidyl methacrylate)s with Controlled Molecular Weights as Low-Shrinkage Resins for 3D Multibeam Interference Lithography. *J. Mater. Chem.* **2008**, *18*, 3316−3318.

(13) Bêche, B.; Pelletier, N.; Gaviot, E.; Zyss, J. Single-Mode TE00-TM00 Optical Waveguides on SU-8 Polymer. *Opt. Commun.* **2004**, *230*, 91−94.

(14) Pelletier, N.; Bêche, B.; Tahani, N.; Zyss, J.; Camberlein, L.; Gaviot, E. SU-8 Waveguiding Interferometric Micro-Sensor for Gage Pressure Measurement. *Sens. Actuators, A* **2007**, *135*, 179−184.

(15) Conradie, E. H.; Moore, D. F. SU-8 thick Photoresist Processing as a Functional Material for MEMS applications. *J. Micromech. Microeng.* **2002**, *12*, 368−374.

(16) Dufour, R.; Dibao-Dina, A.; Harnois, M.; Tao, X.; Dufour, C.; Boukherroub, R.; Senez, V.; Thomy, V. Electrowetting on Functional Fibers. *Soft Matter* **2013**, *9*, 492−497.

(17) Jacques, E.; Romain, M.; Yassin, A.; Bebiche, S.; Harnois, M.; Mohammed-Brahim, T.; Rault-Berthelot, J.; Poriel, C. An Electron Deficient Dicyanovinylene-Ladder-Type Pentaphenylene Derivative for n-Type Organic Field Effect Transistors. *J. Mater. Chem. C* **2014**, *2*, 3292−3302.

(18) Shirtcliffe, N. J.; Aqil, S.; Evans, C.; McHale, G.; Newton, M. I.; Perry, C. C.; Roach, P. The Use of High Aspect Ratio Photoresist (SU-8) for Super-Hydrophobic Pattern Prototyping. *J. Micromech. Microeng.* **2004**, *14*, 1384−1389.

(19) Jiguet, S.; Bertsch, A.; Hofmann, H.; Renaud, P. SU8-Silver Photosensitive Nanocomposite. *Adv. Eng. Mater.* **2004**, *6*, 719−724.

(20) Chen, W. C.; Wu, T. J.; Wu, W. J.; Su, G.D. J. Fabrication of Inkjet-Printed SU-8 Photoresist Microlenses Using Hydrophilic Confinement. *J. Micromech. Microeng.* **2013**, *23*, 065008−065016.

(21) Voigt, A.; Ostrzinski, U.; Pfeiffer, K.; Kim, J. Y.; Fakhfouri, V.; Brugger, J.; Gruetzner, G. New Inks for the Direct Drop-on-Demand Fabrication of Polymer Lenses. *Microelectron. Eng.* **2011**, *88*, 2174−2179.

(22) Mionić, M.; Pataky, K.; Gaal, R.; Magrez, A.; Brugger, J.; Forró, L. Carbon Nanotubes−SU8 Composite For Flexible Conductive Inkjet Printable Applications. *J. Mater. Chem.* **2012**, *22*, 14030−14034.

(23) Fromm, J. E. Numerical Calculation of the Fluid Dynamics of Drop-on-Demand Jets. *IBM J. Res. Dev.* **1984**, *28*, 322−333.

(24) Reis, N.; Derby, B. Ink Jet Deposition of Ceramic Suspensions: Modeling and Experiments of Droplet Formation. *MRS Online Proc. Libr.* **2000**, *625*, null−null.

(25) Jang, D.; Kim, D.; Moon, J. Influence of Fluid Physical Properties on Ink-Jet Printability. *Langmuir* **2009**, *25*, 2629−2635.

(26) Tai, J.; Gan, H. Y.; Liang, Y. N.; Lok, B. K. , Control of Droplet Formation in Inkjet Printing Using Ohnesorge Number Category: Materials and Processes; 10th Electronics Packaging Technology Conference; EPTC: Singapore, 2008; pp 761−766.

(27) Derby, B. Inkjet Printing of Functional and Structural Materials: Fluid Property Requirements, Feature Stability, and Resolution. *Annu. Rev. Mater. Res.* **2010**, *40*, 395−414.

(28) Nallan, H. C.; Sadie, J. A.; Kitsomboonloha, R.; Volkman, S. K.; Subramanian, V. Systematic Design of Jettable Nanoparticle-Based Inkjet Inks. *Langmuir* **2014**, *30*, 13470−13477.

(29) Fakhfouri, V.; Mermoud, G.; Kim, J. Y.; Martinoli, A.; Brugger, J. Drop-On-Demand Inkjet Printing of SU-8 Polymer. *Micro Nanosyst.* **2009**, *1*, 63−67.

(30) Kawase, T.; Sirringhaus, H.; Friend, R. H.; Shimoda, T. Inkjet Printed Via-Hole Interconnections and Resistors for All-Polymer Transistor Circuits. *Adv. Mater.* **2001**, *13*, 1601−1605.

(31) Soltman, D.; Subramanian, V. Inkjet-Printed Line Morphologies and Temperature Control of the Coffee Ring Effect. *Langmuir* **2008**, *24*, 2224−2231.

(32) Duineveld, P. C. The stability of ink-jet Printed Lines of Liquid With Zero Receding Contact Angle on a Homogeneous Substrate. *J. Fluid Mech.* **2003**, *477*, 175−200.

(33) Liu, M.; Wang, J.; He, M.; Wang, L.; Li, F.; Jiang, L.; Song, Y. Inkjet Printing Controllable Footprint Lines by Regulating the Dynamic Wettability of Coalescing Ink Droplets. *ACS Appl. Mater. Interfaces* **2014**, *6*, 13344−13348.

(34) Anyfantakis, M.; Baigl, D. Dynamic Photocontrol of the Coffee-Ring Effect with Optically Tunable Particle Stickiness. *Angew. Chem., Int. Ed.* **2014**, *53*, 14077−14081.

(35) Cui, L. Y.; Li, Y. F.; Wang, J. X.; Tian, E. T.; Zhang, X. Y.; Zhang, Y. Z.; Song, Y. L.; Jiang, L. Fabrication of large-area patterned photonic crystals by ink-jet printing. *J. Mater. Chem.* **2009**, *19*, 5499−5502.

(36) Kim, D.; Jeong, S.; Park, B. K.; Moon, J. Direct writing of silver conductive patterns: Improvement of film morphology and conductance by controlling solvent compositions. *Appl. Phys. Lett.* **2006**, *89*, 264101.

(37) Hu, H.; Larson, R. G. Marangoni Effect Reverses Coffee-Ring Depositions. *J. Phys. Chem. B* **2006**, *110*, 7090−7094.

(38) Shaw, M.; Nawrocki, D.; Hurditch, R.; Johnson, D. Processing of Thin SU-8 Films. *Microsyst. Technol.* **2003**, *10*, 17−21.

(39) Tekin, E.; De Gans, B. J.; Schubert, U. S. Ink-Jet Printing of Polymers − from Single Dots to Thin Film Libraries. *J. Mater. Chem.* **2004**, *14*, 2627−2632.

(40) Van den Berg, A. M. J.; De Laat, A. W. M.; Smith, P. J.; Perelaer, J.; Schubert, U. S. Geometric Control of Inkjet Printed Features Using a Gelating Polymer. *J. Mater. Chem.* **2007**, *17*, 677−683.

(41) Tetzner, K.; Bose, I. R.; Bock, K. Organic Field-Effect Transistors Based on a Liquid-Crystalline Polymeric Semiconductor using SU-8 Gate Dielectrics on Flexible Substrates. *Materials* **2014**, *7*, 7226−7242.

(42) Fukuda, K.; Sekine, T.; Kumaki, D.; Tokito, S. Profile Control of Inkjet Printed Silver Electrodes and Their Application to Organic Transistors. *ACS Appl. Mater. Interfaces* **2013**, *5*, 3916−3920.

(43) Facchetti, A.; Yoon, M. H.; Marks, T. J. Gate Dielectrics for Organic Field-Effect Transistors: New Opportunities for Organic Electronics. *Adv. Mater.* **2005**, *17*, 1705−1725.

(44) Mamada, M.; Shima, H.; Yoneda, T.; Shimano, T.; Yamada, N.; Kakita, K.; Machida, T.; Tanaka, Y.; Aotsuka, Y.; Kumaki, D.; Tokito, S. A Unique Solution-Processable n-Type Semiconductor Material Design for High-Performance Organic Field-Effect Transistors *Chem. Mater.* **2015**, *27*, 141−147.

(45) Maverick, A.; Gray, W. Luminescence and Redox Photochemistry of the Molybdenum(II) Cluster Mo6Cl142-. *J. Am. Chem. Soc.* **1981**, *103*, 1298−1300.

(46) Cordier, S.; Grasset, F.; Molard, Y.; Amela-Cortes, M.; Boukherroub, R.; Ravaine, S.; Mortier, M.; Ohashi, N.; Saito, N.; Haneda, H. Inorganic Molybdenum Octahedral Nanosized Cluster Units, Versatile Functional Building Block for Nanoarchitectonics. *J. J. Inorg. Organomet. Polym. Mater.* **2015**, *25*, 189−204.

(47) Ariga, K.; Ji, Q.; Nakanishi, W.; Hill, J. P. Thin Film Nanoarchitectonics. *J. Inorg. Organomet. J. Inorg. Organomet. Polym. Mater.* **2015**, *25*, 466.

(48) Cordier, S.; Molard, Y.; Brylev, K.; Mironov, Y.; Grasset, F.; Fabre, B.; Naumov, N. Advances in the Engineering of Near Infrared Emitting Liquid Crystals and Copolymers, Extended Porous Frameworks, Theranostic Tools and Molecular Junctions Using Tailored Re6 Cluster Building Blocks. *J. Cluster Sci.* **2015**, *26*, 53−81.

(49) Cordier, S.; Dorson, F.; Grasset, F.; Molard, Y.; Fabre, B.; Haneda, H.; Sasaki, T.; Mortier, M.; Ababou-Girard, S.; Perrin, C. Novel Nanomaterials Based on Inorganic Molybdenum Octahedral Clusters. *J. Cluster Sci.* **2009**, *20*, 9−21.

(50) Molard, Y.; Dorson, F.; Circu, V.; Roisnel, T.; Artzner, F.; Cordier, S. Clustomesogens: Liquid Crystal Based Transition Metal Clusters. *Angew. Chem., Int. Ed.* **2010**, *49*, 3351−3355.

(51) Molard, Y.; Ledneva, A.; Amela-Cortes, M.; Circu, V.; Naumov, N. G.; Meriadec, C.; Artzner, F.; Cordier, S. Ionically Self Assembled Clustomesogen with Switchable Magnetic/Luminescence Properties Containing [Re6Se8(CN)6]n- (n = 3, 4) Anionic Clusters. *Chem. Mater.* **2011**, *23*, 5122−5130.

(52) Nayak, S. K.; Amela-Cortes, M.; Roiland, C.; Cordier, S.; Molard, Y. From Metallic Cluster-based Ceramics to Nematic Hybrid Liquid Crystals: A Double Supramolecular Approach. *Chem. Commun.* **2015**, *51*, 3774−3777.

(53) Amela-Cortes, M.; Garreau, A.; Cordier, S.; Faulques, E.; Duvail, J. L.; Molard, Y. Hexacyano Octahedral Metallic Clusters as Versatile Building Blocks in the Design of Extended Polymeric Framework and Clustomesogens. *J. Mater. Chem. C* **2014**, *2*, 1545−1552.

(54) Molard, Y.; Labbe, C.; Cardin, J.; Cordier, S. Sensitization of Er3+ Infra-red Photoluminescence Embedded in an Hybrid Organic-Inorganic Copolymer Containing Octahedral Molybdenum Clusters. *Adv. Funct. Mater.* **2013**, *23*, 4821−4825.

(55) Sokolov, M. N.; Mihailov, M. A.; Peresypkina, E. V.; Brylev, K. A.; Kitamura, N.; Fedin, V. P. Highly Luminescent Complexes [Mo6 × 8(n-C3F7COO)6]2− (X = Br, I). *Dalton Trans.* **2011**, *40*, 6375−6377.

(56) Kirakci, K.; Kubat, P.; Dusek, M.; Fejfarova, K.; Sicha, V.; Mosinger, J.; Lang, K. A Highly Luminescent Hexanuclear Molybdenum Cluster − A Promising Candidate Toward Photoactive. Materials. *Eur. J. Inorg. Chem.* **2012**, *2012*, 3107−3111.

(57) Kirakci, K.; Cordier, S.; Perrin, C. Synthesis and Characterization of Cs2Mo6 × 14 (X = Br or I) Hexamolybdenum Cluster Halides: Efficient Mo6 Cluster Precursors for Solution Chemistry Syntheses. *Z. Anorg. Allg. Chem.* **2005**, *631*, 411−416.

(58) Amela-Cortes, M.; Paofai, S.; Cordier, S.; Folliot, H.; Molard, Y. Tuned red NIR Phosphorescence of Polyurethane Hybrid Composites Embedding Metallic Nanoclusters for Oxygen Sensing. *Chem. Commun.* **2015**, *51*, 8177−8180.

(59) Amela-Cortes, M.; Garreau, S.; Cordier, S.; Faulques, E.; Duvail, J. L.; Molard, Y. Deep red luminescent hybrid copolymer materials with high transition metal cluster content. *J. Mater. Chem. C* **2014**, *2*, 1545−1552.

(60) Xun, S.; Meng, H.; Wudl, F.; Perepichka, D. F.; Perepichka, I. F. Light emitting polymers. In *Organic Light-Emitting Materials and Devices*, 2nd ed.; CRC Press: Boca Raton, 2015; Vol 180, p 41; DOI: 10.1201/b18540-3.

(61) Huang, F.; Hou, L.; Shen, H.; Jiang, J.; Wang, F.; Zhen, H.; Cao, Y. Synthesis, photophysics, and electroluminescence of high-efficiency saturated red light-emitting polyfluorene-based polyelectrolytes and their neutral precursors. *J. Mater. Chem.* **2005**, *15*, 2499−2507.

(62) Wood, S. M.; Prévôt, M.; Amela-Cortes, M.; Cordier, S.; Elston, S. J.; Molard, Y.; Morris, S. M. Polarized phosphorescence of isotropic and metal-based clustomesogens dispersed into chiral nematic liquid crystalline films, Adv. *Adv. Opt. Mater.* **2015**, n/a.